Pattern Recognition 43 (2010) 3879–3890

Contents lists available at ScienceDirect

Pattern Recognition

journal homepage: www.elsevier.com/locate/pr

Pixel-level singular point detection from multi-scale Gaussian filtered orientation field

Changlong Jin, Hakil Kim *

School of Information and Communication Engineering, INHA University, Republic of Korea

ARTICLE INFO

Article history:
Received 27 October 2009
Received in revised form
12 May 2010
Accepted 18 May 2010

Keywords:
Fingerprint recognition
Gaussian filter
Orientation field
Singular point
Angular gradient
Poincare index

ABSTRACT

Singular point, as a global feature, plays an important role in fingerprint recognition. Inconsistent detection of singular points apparently gives an affect to fingerprint alignment, classification, and verification accuracy. This paper proposes a novel approach to pixel-level singular point detection from the orientation field obtained by multi-scale Gaussian filters. Initially, a robust pixel-level orientation field is estimated by a multi-scale averaging framework. Then, candidate singular points in pixel-level are extracted from the complex angular gradient plane derived directly from the pixel-level orientation field. The candidate singular points are finally validated via a cascade framework comprised of nested Poincare indices and local feature-based classification. Experimental results over the FVC 2000 DB2 confirm that the proposed method achieves robust and accurate orientation field estimation and consistent pixel-level singular point detection. The experimental results exhibit a low computational cost with better performance. Thus, the proposed method can be employed in real-time fingerprint recognition.

© 2010 Elsevier Ltd. All rights reserved.

1. Introduction

Singular point (SP), as an important global feature of fingerprint, can be utilized to index the fingerprint in large-scale databases, so as to limit the search space [1–6]. It can be used to reconstruct a fingerprint from a template [7], to model the orientation field (OF) [8,9], or to align the enrolled template to the input fingerprint in fingerprint pattern matching [5,10]. Consistent SPs increase the accuracy of fingerprint classification [6] and the performance of fingerprint matching [10].

SP is classified as core and delta and it has two definitions, Henry's definition [11] and OF-based definition. Henry defines the core as the topmost point of the innermost curving ridge, and delta as the center of a triangular region, where three different ridge flows meet. The SPs should be located on the ridge lines. This definition coincides with ISO/IEC 19794-2 [12]. On the other hand, automatic SP detection methods [1,8,9,13–22] define the SPs as the discontinuous points in OF. While both of these definitions can be used in practice, Henry's definition is commonly used in finding a reference point manually in evaluating the performance of SP detection [15,19]. However, the true position of SP is often difficult to determine manually, even by experts. People may comprehend this definition differently in practice.

Fig. 1b compares Henry's definition-based SP (HDSP) with the OF-based SP (OFSP). HDSP is located somewhere within a circle centered at the ideal SP while OFSP obtained by the proposed method is labeled as the black square above the circle. Since, in general, the OFSP is not completely identical with the HDSP in the coordinates of SP due to the smoothing procedures [3,6,23,24], there exists a tradeoff between coordinates excursion and smoothing effects. Furthermore, the important issue in both definitions is the robustness and the consistency of the detected SPs.

Many approaches of SP extraction are found in the literatures and these approaches can be categorized into Poincare index-based and non-Poincare index-based approaches. The Poincare index (PI), introduced by Kawagoe et al. [4], is the classical way to detect and verify SPs. In this method, the summation of the difference in angle in adjacent vectors, which are associated along with a certain contour, will have special values for SPs and normal points. However, the performance of this method severely depends on the OF estimation. Furthermore, due to the homogenous problem in OF estimation, the single PI-based method has limitation in discriminating false SPs from true ones. The non-PI-based approaches utilize various techniques such as orientation curvature [14,15,21,22], template matching [13,19], and others [1,16,17]. Compared with these latter approaches, PI-based approaches are more robust to image rotation.

Since automatic SP detection is defined in OF, the performance (including both detection error rate and consistency regarding position of SP) of SP detection depends on the OF estimation.

* Corresponding author.
E-mail addresses: cljin@vision.inha.ac.kr (C. Jin), hikim@inha.ac.kr (H. Kim).

0031-3203/$ - see front matter © 2010 Elsevier Ltd. All rights reserved.
doi:10.1016/j.patcog.2010.05.023

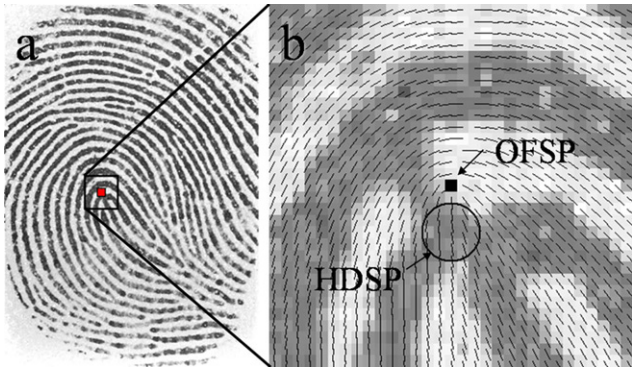

Fig. 1. Comparison between Henry's definition-based SP and orientation field-based SP, (a) the original fingerprint image, (b) Singular area superimposed with pixel-wise OF.

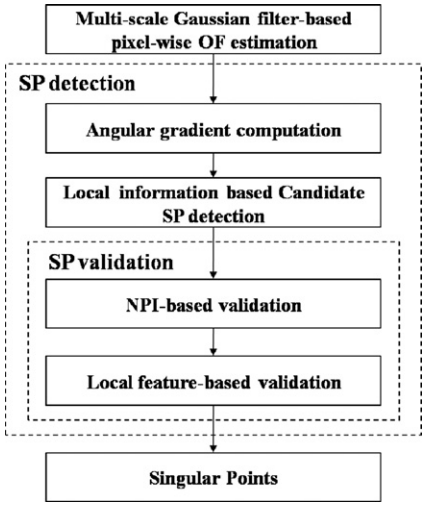

Fig. 2. The flowchart of proposed SP detection.

The existing methods of SP detection except the PCA-based approach [18] are based on block-wise OF, thus, the resolution and consistency of SP is limited by the block size in OF estimation since decreasing the block size will introduce much noise. Moreover, the block-wise OF is difficult in finding close SPs, such as two close cores and core-delta pair. The PCA-based method can compute pixel-wise OF using a linear filtering technique, however, the application of single linear filter limits the accuracy of OF estimation, consequently produces many false SPs (refer to Table 2 for comparison).

Motivated by the need to compute consistent pixel-level SPs with a low detection error rate, in this paper, firstly, a robust pixel-wise OF is computed based on multi-scale Gaussian filter. Secondly, the candidate SPs are extracted in the pixel-wise complex angular gradient plane derived from the prior OF. Finally, nested Poincare indices (NPI) and local feature-based classification are used to verify the candidate SPs and to remove the false SPs from the candidate SPs. Fig. 2 shows the flowchart of the proposed SP detection.

Since the OF estimation is based on multi-scale Gaussian filter, the obtained OF has the advantages: (i) robust to local defects, (ii) a pixel-wise OF, thus, pixel-level SPs, (iii) increase in the matching performance [25], and (iv) fewer number of discontinuous points (candidate SPs). Furthermore, the error rate in SP detection is significantly reduced by the cascade framework comprised of NPI in OF domain and local feature-based classification. In addition, in order to remove the subjective evaluation on the performance of SP detection results, a cross correlation matching (CCM)-based method is employed and thus results in objective performance evaluation, whereas the existing methods [15,19] use manually detected SP as the reference point to evaluate the performance of SP detection.

2. Pixel-wise orientation field estimation

A reliable pixel-wise OF estimation method is of primary importance in pixel-level SP detection because automatically detected SPs are defined as the discontinuous points in the OF. Robust high resolution OF not only enhances the accuracy in position of SPs but also reduces the number of false SPs. Brief introduction of the pixel-wise OF estimation method was previously published in Ref. [25]. This paper provides more detailed mathematical derivation with an example.

2.1. Related works

Several OF estimation approaches have been developed. These approaches can be broadly categorized into four classes: filter-bank-based approach, model-based approach, PCA-based approach, and gradient-based approach. The filter-bank-based approaches [3,6,22,23] estimate the OF based on pixel alignments with respect to a fixed number of orientation masks. Park et al. [2] propose a modified filter-bank which plays a role of a low-pass filter in the frequency domain. The accuracy of the estimated results in the filter-bank-based approach is limited due to the fixed number of reference orientations, block-wise mode, and sensitivity to noise.

Model-based approaches have attempted to model the OF mathematically by taking the global information [8,9,16], quadratic differentials [26], polynomial fitting [27], Markov random field [20], or 2-D Fourier expansion [17]. Model-based approaches are not suitable in finding consistent high resolution SPs because: (i) they need prior-knowledge regarding SP or tradeoff between miss-estimation on good quality areas and the prediction on low quality areas and (ii) the modeled OF has difficulty in representing slight changes in orientation and abrupt changes in SP areas.

Bazen et al. [18] propose a PCA-based approach, which has been proven mathematically equivalent to the conventional squared gradient-based methods, and a modified multi-scale-based approach [28]. Even though this approach produces a pixel-wise OF, it is still sensitive to noise due to insufficient smoothing operation.

The gradient-based approach proposed by Rao et al. [29] has been most widely used in the computation of the dominant orientation of fingerprint images [1,5,14,15,24,30,31]. The orientation of a block in fingerprint is estimated by averaging the squared gradients to avoid directional ambiguity. Several modified gradient-based approaches have been proposed in the literature. Mei et al. [30] estimate the OF in multi-size blocks based on the curvature measure. Wang et al. [31] propose another modified scheme of this conventional squared gradient-based method, where the orientation of a central block is selected by the best orientation from four overlapping neighborhoods that are decided by the coherence measure of each block. The limitations of these gradient-based approaches result from the block-wise mode. It is hard to extract consistent pixel-level SPs from the block-wise OF. Furthermore, due to the presence of noise, corrupted ridge/valley structures, minutiae, etc., the estimated OF is not always accurate. In order to overcome these weaknesses in gradient-based approaches, the multi-scale Gaussian filter-based OF estimation has been proposed in Ref. [25]. This approach is described in more detail in the following sub-section.

2.2. Qualitative analysis

In detection of ridge orientation, there is always an ambiguity of deciding the orientation as either θ or $\theta+\pi$. In order to solve this ambiguity, Rao et al. [29] propose a method, so called, squared gradient, by doubling the angles of the gradient vectors before averaging. It is demonstrated that the square of gradient vectors pointing to opposite directions makes them reinforce each other. The squared gradient can be expressed in terms of G_x and G_y by

$$G_{s,x}+jG_{s,y}=(G_x+jG_y)^2=(G_x^2-G_y^2)+j(2G_{xy}), \tag{1}$$

where G_x^2, G_{xy}, and G_y^2 refer to multiplication of G_xG_x, G_xG_y, and G_yG_y, respectively. Also, the orientation at each pixel (x,y) can be computed by $\theta=(1/2)\tan^{-1}(G_{s,y}/G_{s,x})+\pi/2$, which can be extended to block-wise computation for smoothing effect in a local area,

$$\theta(x_b,y_b)=(1/2)\tan^{-1}\left(\sum_{w\times w}G_{s,y}(x,y)/\sum_{w\times w}G_{s,x}(x,y)\right)+\pi/2, \tag{2}$$

where w and (x_b, y_b) refer to the block size and the block center, respectively. Most of the research works [1,5,14,15,24,30,31] for OF estimation adopt this scheme by summing the components of the squared gradient in a block, as Eq. (2) shows, and thus result in a block-wise OF rather than pixel-wise OF.

In this paper, the coherence data, G_x^2, G_y^2, and G_{xy}, which are the components of the squared gradient, are convoluted by a block-scale Gaussian filter instead of block-wise summation, thus resulting in a pixel-wise squared gradient and pixel-wise OF. This method is similar to the PCA-based method in terms of the pixel-level OF estimation, but includes a smoothing process of multi-scale low pass filtering on three different scales, consequently, produces more robust and accurate OF (refer to Fig. 14 for qualitative comparison).

2.3. Quantitative derivation

The pixel-wise OF estimation consists of three-stage filtering in three scales, namely, gradient vectors smoothing in pixel-scale, coherence data smoothing in block-scale, and sinusoidal components smoothing in orientation-scale. The rationale behind this is the same with the conventional squared gradient-based method. However, the difference is that the convolution operation which utilizes the advantage of Gaussian function takes the place of the block summation and post smoothing procedure [24], thus results in robust pixel-wise OF which is beneficial to reduce the number of the candidate SPs and enhance the consistency of SPs.

2.3.1. Gradient vectors smoothing in pixel-scale

Fingerprint images usually contain noise due to perspiration, dirt, scars, smudges, sensor noise, etc. Since these noise make the gradient vectors chaotic, a low pass filter is essential to reduce the noise and obtain the smoothed gradient vectors. The Gaussian filter is the most widely used low-pass filter due to its excellent features of Gaussian function. The general case of an isotropic Gaussian filter in 2-D space is denoted as $g(x,y,\sigma_i)$, where $\sigma_i(i=1,2,3)$ refer to the variances in three different scales. The gradient vectors smoothed in pixel-level can be computed by

$$\begin{bmatrix}G_x(x,y)\\G_y(x,y)\end{bmatrix}=\begin{bmatrix}(\partial g(x,y,\sigma_1)/\partial x)*I(x,y)\\(\partial g(x,y,\sigma_1)/\partial y)*I(x,y)\end{bmatrix}, \tag{3}$$

where the asterisk ($*$) denotes the convolution with the input image $I_{M\times N}$. Fig. 3b and c shows the smoothed gradient vector fields in gray-level images.

2.3.2. Coherence data smoothing in block-scale

In general, the components of the squared gradient in Eq. (1), G_x^2, G_y^2, and G_{xy}, are derived from the coherence matrix $\mathbf{C}$ by block-wise summation,

$$\mathbf{C}_{M/w\times N/w}=\{\mathbf{C}_{ij}\}, \tag{4}$$

where

$$\mathbf{C}_{ij}=\sum_{w\times w}\begin{bmatrix}G_x(x,y)\\G_y(x,y)\end{bmatrix}[G_x(x,y)\;\;G_y(x,y)]$$
$$=\sum_{w\times w}\begin{bmatrix}G_x^2(x,y) & G_{xy}(x,y)\\G_{xy}(x,y) & G_y^2(x,y)\end{bmatrix}.$$

Instead of a simple summation in Eq. (4), a low-pass filter can be applied to perform a weighted summation of the coherence data,

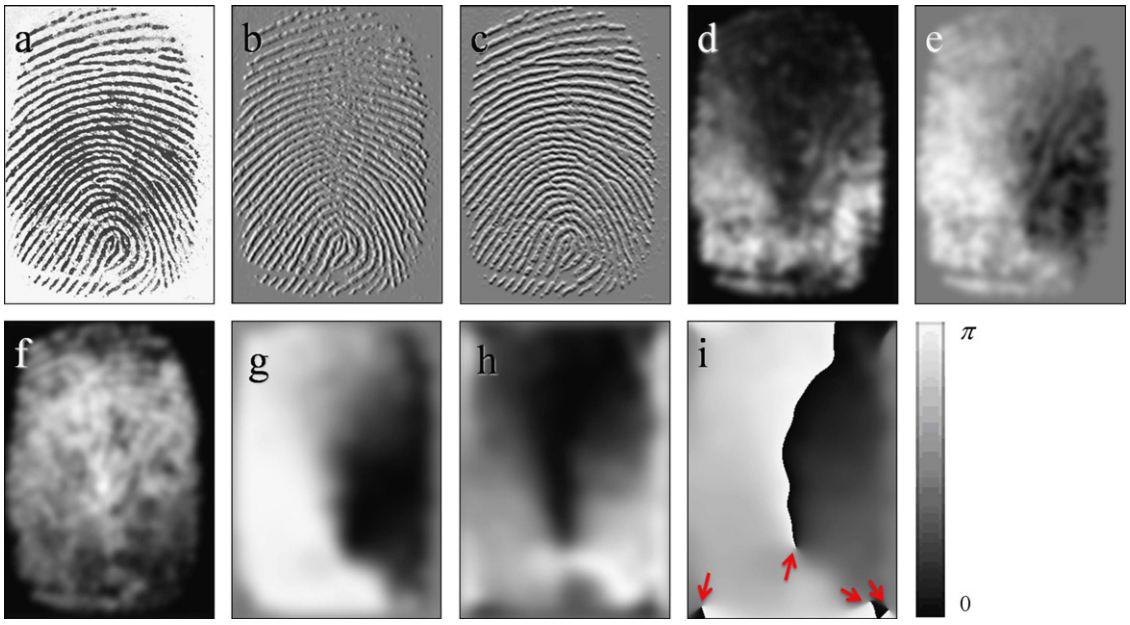

Fig. 3. Intermediate results of the pixel-wise OF estimation: (a) original fingerprint image, (b) G_x, (c) G_y, (d) G_{gx}^2, (e) G_{gxy}, (f) G_{gy}^2, (g) $\sin_g(\phi(x,y))$, (h) $\cos_g(\phi(x,y))$, and (i) gray-scale coded OF with the legend, and the arrows point to the four discontinuous points in OF domain.

$G_x^2(x,y)$, $G_y^2(x,y)$, and $G_{xy}(x,y)$. In this study, the pixel-wise coherence matrix is computed by convolution of the gradient vectors smoothed in pixel-scale with a Gaussian filter in block-scale, as shown

$$\mathbf{C}_{M\times N} = \{\mathbf{C}_{ij}\}, \tag{5}$$

where

$$\mathbf{C}_{ij} = \begin{bmatrix} G_{gx}^2(x,y) & G_{gxy}(x,y) \\ G_{gyx}(x,y) & G_{gy}^2(x,y) \end{bmatrix} = \begin{bmatrix} g(x,y,\sigma_2) * G_x^2(x,y) & g(x,y,\sigma_2) * G_{xy}(x,y) \\ g(x,y,\sigma_2) * G_{yx}(x,y) & g(x,y,\sigma_2) * G_y^2(x,y) \end{bmatrix}.$$

Thus, the squared gradient, $[G_{gs,x}G_{gs,y}]^T$ (the real part and the image part of Eq. (1)) can be derived from the filtered coherence matrix as follows:

$$\begin{bmatrix} G_{gs,x}(x,y) \\ G_{gs,y}(x,y) \end{bmatrix} = \begin{bmatrix} G_{gx}^2(x,y) - G_{gy}^2(x,y) \\ 2G_{gxy}(x,y) \end{bmatrix}. \tag{6}$$

Fig. 3 d, e and f shows the components of the filtered coherence matrix.

2.3.3. Sinusoidal components smoothing in orientation-scale

Even though a pixel-wise OF can be obtained from the filtered squared gradient as

$$\theta(x,y) = (1/2)\tan^{-1}(G_{gs,y}(x,y)/G_{gs,x}(x,y)) + \pi/2, \tag{7}$$

the resulted OF is still likely to yield false discontinuous points due to insufficient smoothing. One solution would be to perform further smoothing with a larger σ_2, which will cause an over-smoothing problem, that is, the OFSP will be shifted too much away from the HDSP.

For the purpose of solving this problem, this study adopts the orientation-scale smoothing which consists of four steps:

(i) The sinusoidal components of the squared gradient are computed for each pixel,

$$\begin{cases} \cos(\phi(x,y)) = G_{gs,x}/\sqrt{G_{gs,x}^2(x,y) + G_{gs,y}^2(x,y)} \\ \sin(\phi(x,y)) = G_{gs,y}/\sqrt{G_{gs,x}^2(x,y) + G_{gs,y}^2(x,y)} \end{cases}, \tag{8}$$

where $\phi(x,y)$ is the doubled angles at each pixel.

(ii) These components are convoluted by an orientation-scale Gaussian filter,

$$\begin{cases} \cos_g(\phi(x,y)) = g(x,y,\sigma_3) * \cos(\phi(x,y)) \\ \sin_g(\phi(x,y)) = g(x,y,\sigma_3) * \sin(\phi(x,y)) \end{cases}. \tag{9}$$

(iii) The doubled angles are computed by

$$\phi(x,y) = \tan^{-1}(\sin_g(\phi(x,y))/\cos_g(\phi(x,y))), \quad -\pi \le \phi < \pi. \tag{10}$$

(iv) The final ridge orientation is derived from Eq. (10) by

$$\theta(x,y) = \phi(x,y)/2 + \pi/2, \quad 0 \le \theta < \pi. \tag{11}$$

Fig. 3g, h and i shows the sinusoidal components and the final pixel-wise OF obtained by the multi-scale Gaussian filtering method. The pixel-wise OF is gray-scale coded, where the angles in the range of 0 to π are linearly mapped to the gray-level from black to white.

Since the multi-scale Gaussian filter-based pixel-wise OF takes the advantages as mentioned in Section 1, very few discontinuous points are produced in the pixel-wise OF. For example, there are only four discontinuous points in Fig. 3i. These points are extracted as the candidate SPs and verified by NPI and local feature-based classification in the next section.

3. Singular points extraction

Unlike the previous SP detection methods discussed in Section 1, this study proposes a coarse-to-fine strategy for SP extraction based on not only the pixel-wise OF but also spatial and spectral features in local areas. Firstly, the candidate SPs are detected by searching the discontinuity of the amplitude in a complex angular gradient plane that is derived from the pixel-wise OF, and then, the candidate SPs are validated via a cascade framework which is comprised of NPI and local feature-based classification trained by spectral and spatial features in a local area around each candidate SP.

3.1. Candidate singular points detection

In order to extract the high resolution candidate SPs, a pixel-wise complex angular gradient plane is computed to detect discontinuous points in OF. The doubled angle ϕ derived from Eq. (10) is used to avoid the intrinsic discontinuity of angles from 0 to π, and transformed into a vector field $V(x,y) = [u(x,y), v(x,y)]^T$, where $u(x,y) = \cos(\phi(x,y))$ and $v(x,y) = \sin(\phi(x,y))$. Then, the angular gradients are derived by the inner product,

$$\begin{cases} \phi'_x(x,y) = \partial\phi(x,y)/\partial x = \cos^{-1}(u(x,y)u(x+1,y) + v(x,y)v(x+1,y)), \\ \phi'_y(x,y) = \partial\phi(x,y)/\partial y = \cos^{-1}(u(x,y)u(x,y+1) + v(x,y)v(x,y+1)). \end{cases} \tag{12}$$

Further, the pixel-wise complex angular gradient plane is constructed by the angular gradients as

$$P_{ag}(x,y) = \phi'_x(x,y) + j\phi'_y(x,y). \tag{13}$$

Since orientations of ridge lines in fingerprint change smoothly except SP areas, the amplitude, $|P_{ag}|$, becomes very small (near zero) for non-SP areas and high peaks for SP areas, as depicted in Fig. 4b. Therefore, the detection of candidate SPs is converted to finding local maxima in the $|P_{ag}|$ plane as

$$sp_c = \underset{(x,y)}{\operatorname{argmax}} |P_{ag}(x,y)|. \tag{14}$$

This process does not need any thresholding because the amplitudes of candidate SPs are much larger than those of non-SP points. Eq. (14) is implemented by searching the local maxima through column, row, up-down, and down-up diagonal. Fig. 4c illustrates the corresponding discontinuous points in OF. There are eight discontinuous points denoted as d_1, d_2, …, d_8, among which d_5, d_6, d_7 and d_8 are false SPs. They will be removed by the validation process described in the next section.

3.2. Singular points validation

The candidate SPs only represent the discontinuous points in the OF. False discontinuous points exist in the detected candidate SPs due to the low quality area in the fingerprint and the homogeneous problem of Eq. (2) (i.e., both denominator and numerator are very small). Therefore, the validation stage is indispensable. All of the false SPs in the candidate SPs can be categorized into two classes: the false SPs with distorted OF (first class) and the false SPs with canonical OF (second class). Fig. 5a–d, e–f and g–h shows the vectorized pixel-wise OF and the corresponding squared pixel-wise OF of the true SPs, the second class false SPs, and the first class false SPs, respectively. Fig. 6 illustrates both the second false SPs and the true SPs in 2- and 3-D images. This study utilizes NPI for the first class false SPs and local feature-based classification for the second class false SPs.

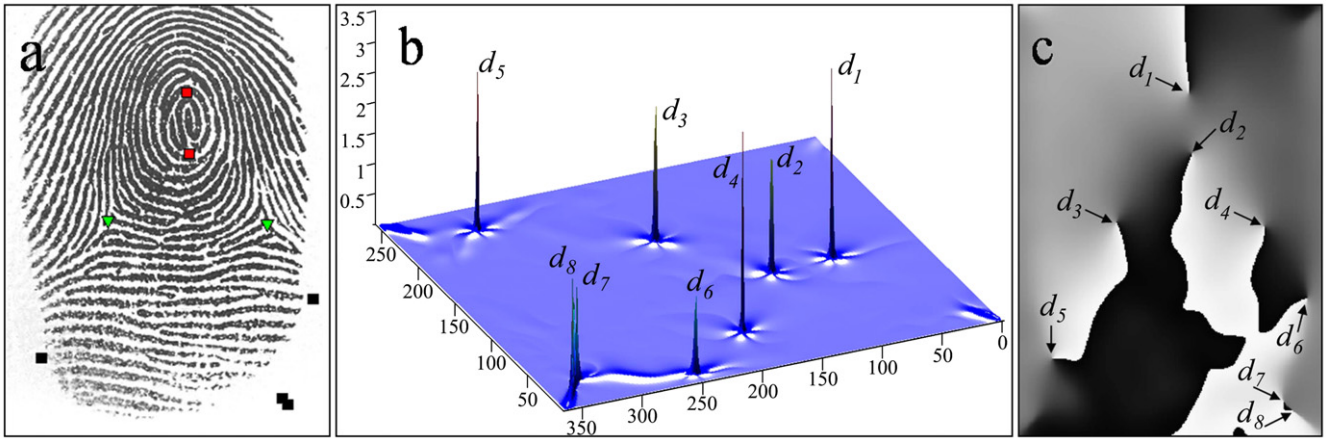

Fig. 4. Candidate SPs detection: (a) original image superimposed with the candidate SPs including four false SPs (■), (b) amplitude plane of the complex angular gradient, and (c) gray-scale coded OF with discontinuous points d_i.

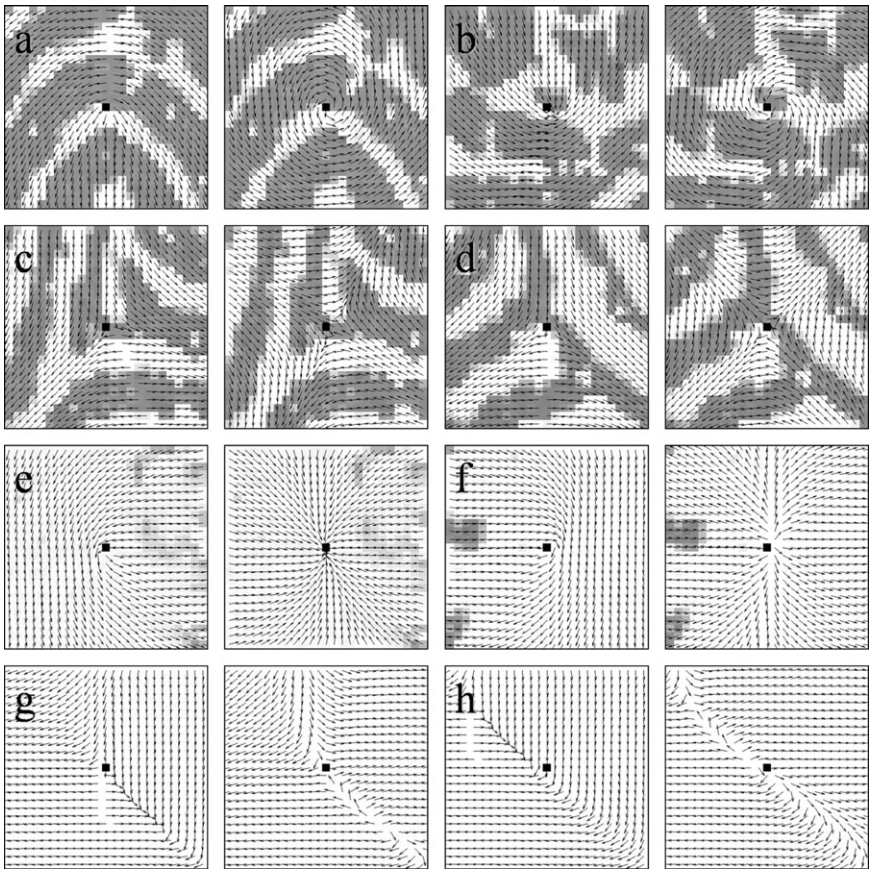

Fig. 5. Vectorized pixel-wise OF and the corresponding squared pixel-wise OF of the candidate SPs superimposed on the local original image: (a) d_1, (b) d_2, (c) d_3, (d) d_4, (e) d_5, (f) d_6, (g) d_7, and (h) d_8.

3.2.1. Nested Poincare indices

The PIs of the closed homotopic paths of a true SP and the second class false SPs are always the same, whereas those of first class false SPs are different. Therefore, the first class false SP can be verified by NPI computed along the closed homotopic paths. Since the multi-scale Gaussian filter-based OF produces pixel-wise OF, applying NPI in a small candidate SP area is possible.

For the purpose of convenience, the PI is generally computed along the perimeter of a square with the target SP located in the center of the square. Furthermore, in order to avoid missing the close SPs, for examples, two close cores and core-delta pairs, the largest contour size should be less than a certain value. For a close core-delta pair shown in Fig. 7, too large square defining a local area may contain more than one SP. Moreover, if two SPs located too close to each other, they can be easily eliminated by NPI, which is a case of arch-type fingerprints. Because the ridge intervals are from 8 to 12 pixels in 500 DPI fingerprint images [32], the largest contour size is selected as so that at most one SP and two ridge lines are contained in the contour, as shown in Fig. 7b.

The procedure of applying NPI to the candidate SPs is as following: eight PI values are computed along with the eight

square contours of different sizes ranging from 3×3 pixels to 17×17 pixels. These PIs are denoted as $\overrightarrow{pi}=\{pi_{3\times3},pi_{5\times5},\ldots,pi_{17\times17}\}$. Then, the standard deviation from the standard PIs is computed by $m_k=\sqrt{(1/(n-1))|\overrightarrow{pi_k}-\overrightarrow{P_s}|^2}$, where $\overrightarrow{P_s}=\{180,180,\ldots,180\}$, n, and k refer to the standard PIs, the number of PI value and the kth candidate SP. Finally, the false SPs are decided by

$$sp_c=\begin{cases}\text{intermediate SPs} & \text{if } m_k<T,\\ \text{false SPs} & \text{otherwise.}\end{cases} \tag{15}$$

The histogram of the m_k is shown in Fig. 8. As can be seen, the values of m_k for false SPs are distributed in a large range whereas those of the true SPs converge around 0°. A few candidate SPs increase as the increase of T, and these candidate SPs are further validated by a local-feature-based classification. The SPs which have distorted OF can be removed by this method, such as d_7 and d_8 in Fig. 5. Then, these intermediate SPs will be verified by the local feature-based classification described in the next subsection.

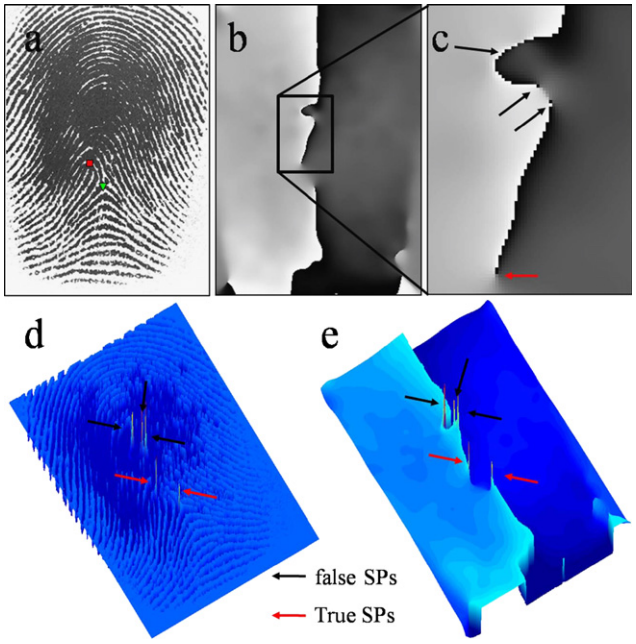

Fig. 6. Examples of the second class false SPs and the true SPs: (a) original fingerprint with smudge area inside, (b) gray-scale coded OF, (c) enlarged gray-scale coded OF, (d) 3-D fingerprint superimposed with the amplitude of complex angular gradient plane, and (e) 3-D gray-scale coded OF.

3.2.2. Local feature-based SP classification

After NPI validation, the first class false SPs can be removed from the candidate SPs. The intermediate SPs contain the true SPs and the second class false SPs, since the second class false SPs have identical vector fields to that of true SPs, it is hard to deal with them further in the OF domain, However, they have different local feature compared to true SPs. These features can be trained and classified by a classifier. When the SP area is transferred into the frequency domain by Fourier transform, the spectral energies of the true SP will contain a strong ring pattern, as shown in Fig. 9c and e. In contrast, the spectral energies of the second class false SPs will concentrate along the and x- and y-axis instead of the ring pattern, as shown in Fig. 9b and f, due to no or weak ridge/valley structures in the local area.

Let $D(x,y)$ denotes the square region of intermediate SP, $1\le(x,y)\le w$, where w is the size of the region. Firstly, $D(x,y)$ is transformed into the frequency domain, $F(\xi,\eta)$, by Fourier transform, and the band energies $E(b)$ ($b=1,\ldots,19$) are computed by the Butterworth band-pass filter [33] over 19 bands which are equi-spaced in the frequency domain. Then, the energies in a band is summed up to form 1-D band energy. If the intermediate SP area contains apparent ridge/valley structure, the middle-frequency bands (from bands 4 to 12), will have high energies compared to low-frequency bands (from bands 1 to 3), whereas the non-ridge/valley structure area will have much lower energies compared to its low-frequency bands. In other words, true SP area has small energies in low-frequency and high energies in

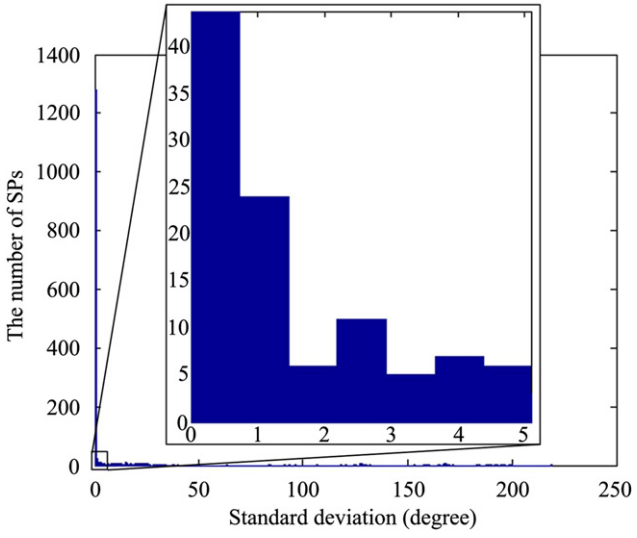

Fig. 8. The histogram of m_k (DB2-a).

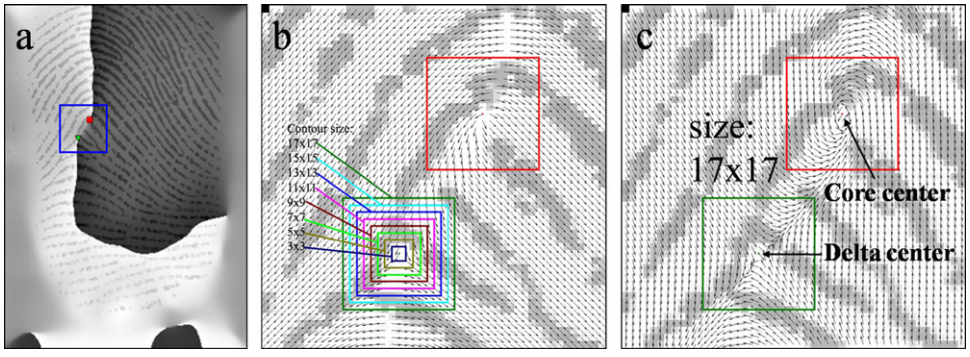

Fig. 7. Close core-delta pair sample: (a) original fingerprint image overlapped with gray-scale coded OF, (b) partial pixel-wise orientation vector field, and (c) partial squared pixel-wise orientation vector field.

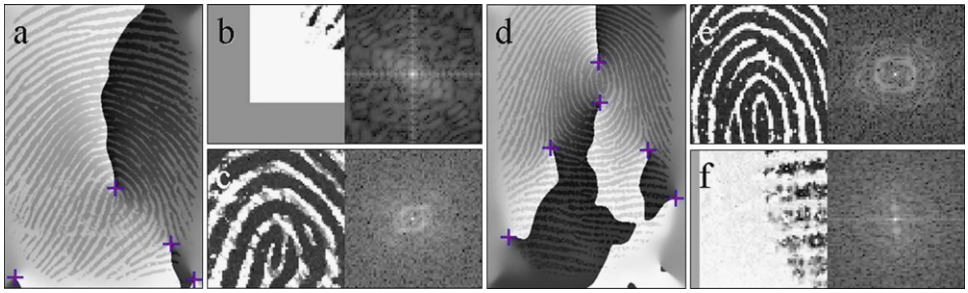

Fig. 9. Sample images with the intermediate SPs and the corresponding Fourier spectral images: (a) and (d) the original sample images overlapped with gray-scale coded OF, the crosses denote the intermediate SPs, (b) and (f) the false SPs located in the foreground boundary and the corresponding Fourier spectral image, (c) and (e) the true SPs and the corresponding Fourier spectral images.

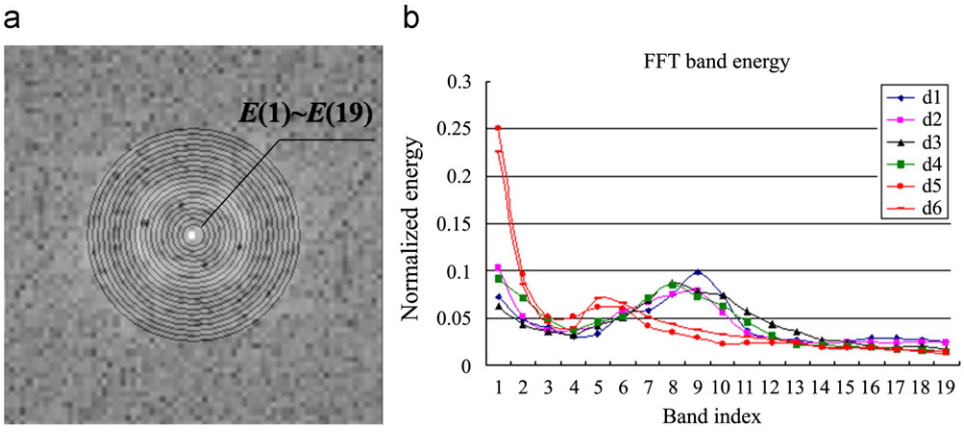

Fig. 10. (a) The band energies $E(b)$, it is corresponding to the curve of d1 in b and (b) distribution of spectral band energies for six discontinuous points in Fig. 9d.

middle-frequency, while the second class false SP has high energies in low-frequency and low energies in middle-frequency. Fig. 10a shows the $E(b)$ and Fig. 10b shows the normalized distributions of $E(b)$, respectively, where the intermediate SPs, d_5 and d_6, are the false SPs so that they have high energies in low-frequency and low energies in middle-frequency. Therefore, the energy ratio of the low-frequency to middle-frequency, as defined in Eq. (16), can be used as the first feature in the spectral domain for the purpose of distinguishing the true SPs from the second class false SPs:

$$r_1 = \sum_{b=1}^{3} E(b) \Big/ \sum_{b=4}^{12} E(b), \tag{16}$$

where $b=1$, 2, 3 are low-frequency bands and $b=4,\ldots,12$ are middle-frequency bands.

The second feature in power spectral domain can be measured by comparing the energy of x- and y-axis to the neighboring energy to check if the energy concentrates along the axes. The sum of the energies that are concentrated along the x- and y-axis is computed as $e_{x,y} = \sum_{\eta=1}^{\eta=w} |F(\xi,\eta)|_{\xi=w/2} + \sum_{\xi=1}^{\xi=w} |F(\xi,\eta)|_{\eta=w/2}$, where w refers to the window size. And, the sum of the neighboring energies that are concentrated on the parallel axes at both sides of the original x- and y-axis is computed as $e_n = \sum_{\eta=1}^{\eta=w} |F(\xi,\eta)|_{\xi=w/2\pm2} + \sum_{\xi=1}^{\xi=w} |F(\xi,\eta)|_{\eta=w/2\pm2}$. Then, the ratio of energy concentration in axes is defined as

$$r_2 = e_{x,y}/e_n. \tag{17}$$

In addition, the standard deviation of the gray-scale values in the false SP area is very small compared to that of true SPs. This feature can be measured by the ratio of a local standard deviation to a foreground standard deviation,

$$r_3 = \sqrt{(1/w)\sum_{x=1}^{w}\sum_{y=1}^{w}(D(x,y)-m_D)^2} \Big/ S_I, \tag{18}$$

where m_D and S_I denote the local mean and the standard deviation of the foreground, respectively. Finally, a vector which represents the local feature is represented as $[r_1, r_2, r_3]^T$ and this is tested by three classical classifiers in Section 4.3.

4. Experiments and discussions

The proposed algorithms have been tested on DB2 of the FVC2000 [34] for the comparison with the previous SP detection approaches [13,15,18,19]. This database contains 880 fingerprint images from 110 individuals (DB2-a with 800 images from 100 individuals, DB2-b with 80 images from 10 individuals), captured by a commercial capacitive sensor with a resolution of 500 DPI. The purpose of the experiments is to show that the proposed algorithms are able to detect robust and consistent singular points in the pixel-level.

4.1. Validation of σ

The σ of a Gaussian filter is an important parameter that can influence the estimated results. When computing a discrete approximation of the Gaussian filter, pixels at a distance of more than are sufficiently small to be considered as effectively zero. Eq. (19) defines the size of the discrete Gaussian filters used in this study in order to ensure the filtered result sufficiently close to

that obtained by the entire Gaussian filter. The filter size is always an odd integer to avoid the bias in discrete computation:

$$s_g = \begin{cases} \lceil 6\sigma \rceil & \text{if mod } (\lceil 6\sigma \rceil, 2) = 1, \\ \lceil 6\sigma \rceil + 1 & \text{otherwise.} \end{cases} \quad (19)$$

The size of the filter in the pixel-level should be less than the ridge interval in order to avoid noise introduced by a neighboring ridge. Since the ridge interval is in general between 8 and 12 pixels for 500 DPI fingerprints [32], an appropriate value of s_g should be less than 8 pixels, which corresponds to $\sigma_1 = 1$. Fig. 11 shows the effect of σ_1 to the gradient flow. It can be observed that the gradient vectors begin to distort in some areas with increasing σ_1.

The second Gaussian filter is used to smooth the coherence data in the block-scale. A higher value for σ_2 in this scale will results in smoother OF because fingerprint has reduplicated structures. However, a larger σ_2 raises two issues in OF estimation. Firstly, while the locations of the OFSP and the HDSP are expected to coincide to each other, a large σ_2 will move OFSP away from the HDSP. Fig. 12 shows that the vector fields become incorrect on the singular area with an increasing σ_2. The second issue is that the runtime tends to increase linearly with the size of the Gaussian filter. Considering these issues, σ_2 is set to a half of the average ridge interval.

Meanwhile, if σ_2 is set to a half of the average ridge interval, the orientation is not smoothed sufficiently and many spurious OF discontinuity points will be resulted in (refer to Fig. 14 for qualitative comparison). Therefore, the filtering in the orientation-scale is indispensable to refrain spurious discontinuity points in OF while keeping the consistency between HDSP and OFSP. In general, it is recommended that σ_3 is twice of σ_2.

4.2. OF verification

Performance of the pixel-wise OF estimation [25] on low quality fingerprints are evaluated and the results show that the pixel-wise OF is accurate and robust. Fig. 13 illustrates the pixel-wise orientation over both minutiae area and local defects such as scar and spot. As shown, the vectorized pixel-wise OF coincides with manual inspection by human vision.

Fig. 14 shows the comparison between the PCA-based method and the proposed method for the fingerprint captured from Ref. [18]. As it shows, Fig. 14b, which is computed by the PCA-based algorithm, is similar to Fig. 14d estimated by the multi-scale Gaussian filter-based method without orientation-scale filtering (due to different coordinate systems, Fig. 14b and d appear differently). There are many discontinuity points in these two sub-figures. Fig. 14c which is estimated by the multi-scale Gaussian filter-based method illustrates a much smoother OF and fewer discontinuity points are produced. This figure demonstrates that the PCA-based method can be further enhanced.

4.3. Statistical performance of singular points extraction

Since the design of classifier is out of the scope of this study, three classical classifiers: back-propagation neural network (BPNN) [35], probabilistic neural network (PNN) [36], and support vector machine (SVM) [37] are employed to test and remove the false SPs based on feature vector, $[r_1, r_2, r_3]^T$, defined in Section 3.2.2. The entire candidate SPs of the dataset, FVC 2000 DB2-b, is used for training set. Fig. 15 shows the training sample distribution in 3-D vector space.

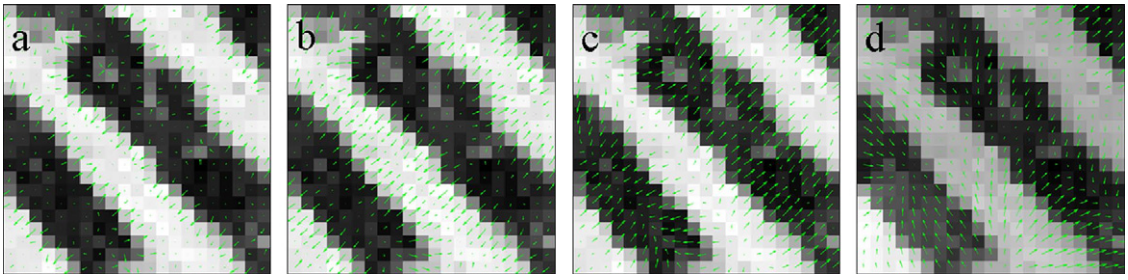

Fig. 11. The effect of σ_1 on gradient vectors: (a) without filtering, (b) $\sigma_1 = 1$, (c) $\sigma_1 = 3$, and (d) $\sigma_1 = 5$.

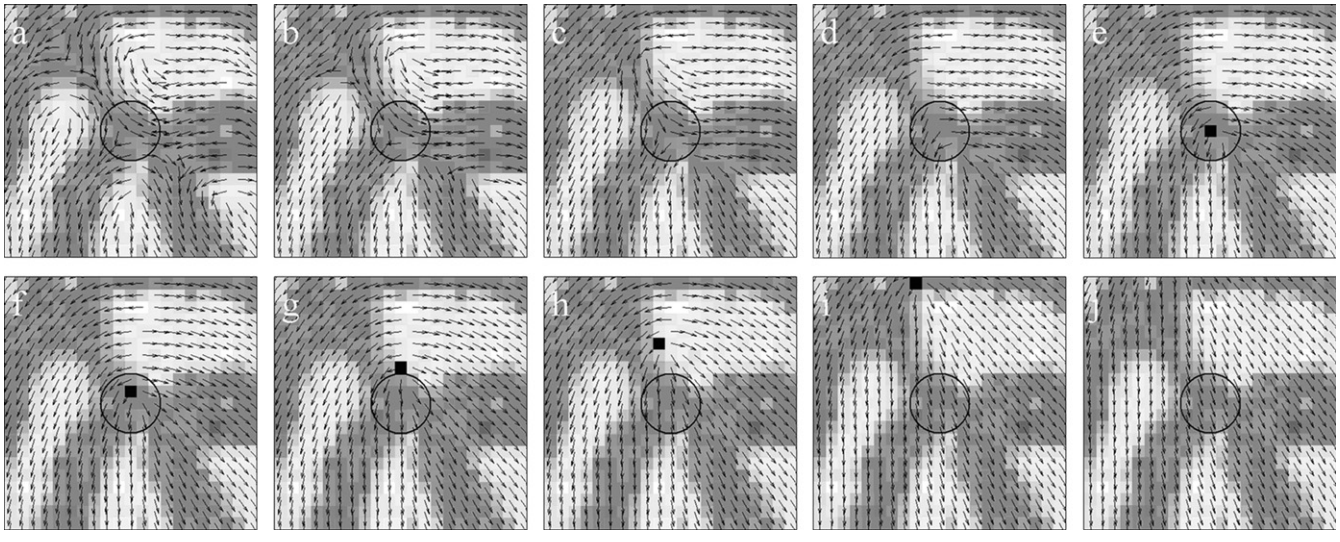

Fig. 12. The effect of σ_2 on SP extraction, $\sigma_1 = 1$ for all OFs, only the σ_2 changes, the center of the circle denotes idea HDSP, and " ■" indicates OFSP: (a) $\sigma_2 = 1$, (b) $\sigma_2 = 2$, (c) $\sigma_2 = 3$, (d) $\sigma_2 = 4$, (e) $\sigma_2 = 5$, (f) $\sigma_2 = 6$, (g) $\sigma_2 = 8$, (h) $\sigma_2 = 10$, (i) $\sigma_2 = 15$, and (j) $\sigma_2 = 19$.

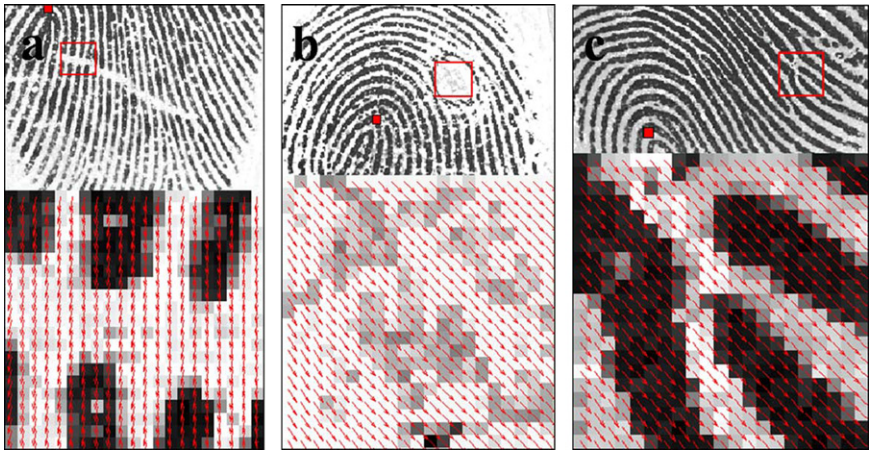

Fig. 13. Examples of pixel-level OF estimation over low-quality fingerprints and minutiae area: (a) wide scar area, (b) circular scar area, and (c) minutiae area.

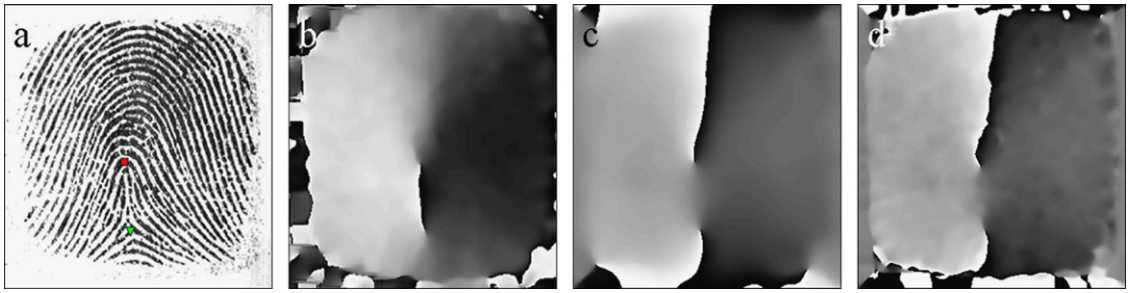

Fig. 14. Comparison of estimated OF: (a) original fingerprint tagged with SPs, (b) OF estimated by PCA-based method, (c) OF estimated by the proposed algorithm with three scale filtering, and (d) OF estimated by the proposed algorithm without orientation-scale filtering.

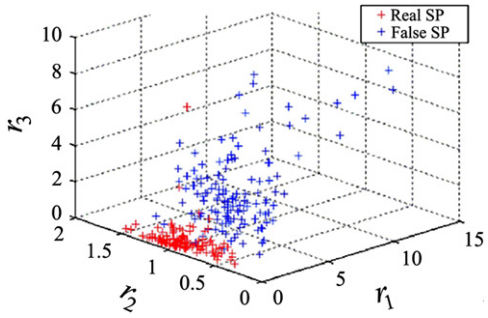

Fig. 15. Distribution of SPs from training samples of FVC 2000 DB2-b.

Table 1
Performance comparison of SP detection over FVC2000 DB2-a (800 fingerprint images).

Method	False SPs	Missed SPs	Total error
Shape analysis-based [15]	45	55	100
Template matching-based [13]	59	69	128
PI-based [15]	181	83	264
Proposed method (NPI+BPNN)	75	13	88
Proposed method (NPI+PNN)	77	9	86
Proposed method (NPI+SVM)	80	7	87

Table 1 shows the performance comparisons of SP detection with the shape analysis-based [15], template matching-based [13], and PI-based methods [15]. The table shows that the proposed method achieves the highest performance with 86 incorrect SPs (PNN classifier) and produces consistently robust results regardless of the type of classifiers. Most of the extraction errors by the proposed method can be attributed to the severe low quality fingerprint images. The largest source of error is due to three bad-quality fingertips: no. 94, no. 97, and no. 100. Thirty-two false SPs are detected from 24 fingerprints that are captured from these three bad-quality fingertips. When the ridge/valley structure is corrupted in a large area, especially in a singularity area, it is hard to extract the correct SPs without global information in such low quality fingerprints.

The results of SP detection of the proposed method and the PCA-based method [18] are reported in Table 2. As seen in this table, the average number of false SPs using the proposed method is significantly fewer than that of the PCA-based method, 84.5% (from 15.4 drop to 2.33, without segmentation) and 78.8% (from 0.8 drop to 0.17, with segmentation) decreases for the set of first-fingerprints (i.e., the dataset comprised of all the first samples of eight fingerprints per individual). The ratio of fingerprints with false SPs using the proposed method is also less than that of PCA-based method. The main reason is due to the smoother OF produced by multi-scale Gaussian filter, thus, fewer spurious discontinuity points are detected in the OF (refer to Fig. 14 for comparison). The other reason is that the nested Poincare indexing is more robust than the single scheme.

Table 2 also shows that the average number of false SPs and the ratio of fingerprints with false SPs of the first-fingerprint set (110 fingerprints) are greater than that of the entire database (880 impressions). It is worth noting that the ratio of fingerprints with missed SPs has 1% (for the first-fingerprint set) and 2% (for the entire database (with segmentation)) errors in the proposed method, respectively.

Table 2
Performance comparison of the proposed SP detection (NPI and BPNN classifier) and the PCA-based method.

Segmentation method and dataset	Proposed method				PCA-based (First-Fp. set)			
	First-Fp.set		Overall dataset					
	(a)	(b)	(c)	(d)	(e)	(f)	(g)	(h)
Average number of false SPs	2.33	0.17	1.96	0.09	15.4	0.8	0.8	0.5
Ratio of fp. with false SPs (%)	90	6	84	5	97	17	20	13
Ratio of fp. with missed SPs (%)	1	1	1	2	0	0	2	5

The proposed SP detection algorithm is implemented: (a) without segmentation, (b) with segmentation over the first-fingerprint set (identical with the PCA-based method, the first-fingerprint set is employed, it contains 110 fingerprints), and (c) without segmentation, (d) with segmentation over the entire DB2 (880 fingerprints). The PCA-based method is implemented: (e) without segmentation, (f) manual segmentation, (g) segmentation algorithm 1, and (h) segmentation algorithm 2 over the first-fingerprint set.

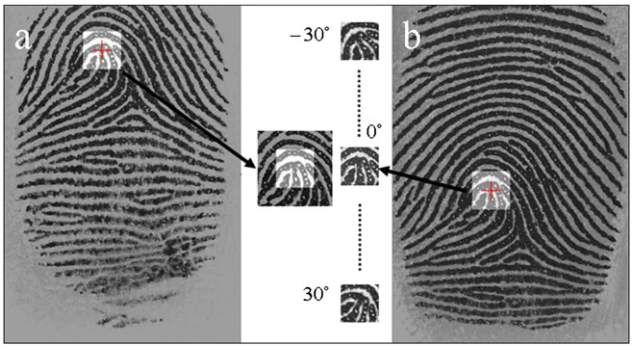

Fig. 16. The CCM-based verification of consistency: (a) the enrolled fingerprint, the light square is the scan region and (b) the tested fingerprint, the light square area is the matched SP region rotated from -30° to 30° degrees, shown in the middle.

4.4. Consistency validation

Consistency has two meanings in this paper. The first indicates the displacement between the HDSPs and the OFSPs. The second refers to the repeatability of the same SPs in different fingerprints from an identical fingertip. This is an important factor in evaluating an SP detection method. A robust OF estimation will result in consistent SPs. The quantitative evaluation of the estimated pixel-wise OF can be made indirectly by the 2nd consistency of detected SPs.

Due to the nonlinear deformation in fingerprints, it is hard to match two identical SP areas of different fingerprints or to figure out by human inspection the amount of translation and rotation between a pair of fingerprints from the same fingertip. Therefore, the matching should be made based on the (CCM) by rotating and translating the tested SP area over the enrolled SP area. As shown in Fig. 16a, a square area of enrolled SP, Z_e, is extracted from the enrolled fingerprint, I_e, where the enrolled SP is located in the center, by

$$Z_e = \{I_e(x,y) | -s \le x - x_{pe} \le s, -s \le y - y_{pe} \le s\}, \quad (20)$$

where s and (x_{pe}, y_{pe}) are the matching range and the coordinates of the enrolled SP, respectively. The computation of the maximum CCM consists of three steps as following:

(i) Extract the same size of tested SP area, Z_t, in which the corresponding SP (x_{pt}, y_{pt}) is located in the center, from the tested fingerprint, I_t, as shown in Fig. 16b, by

$$Z_r = \{I_t(x,y) | -s \le x - x_{pt} \le s, -s \le y - y_{pt} \le s\}. \quad (21)$$

(ii) Compute the CCM by both translating and rotating the matching area to find the maximum CCM.

(iii) The corresponding rotated angle and the shift are recorded. The shift refers to the displacement between the enrolled SP and the tested SP.

This experiment is implemented in all non-arch type fingerprints (696 out of 800 fingerprints in DB2-a), and yielded 914 trials for all extracted SP pairs. Fig. 17a shows the distribution of shifts in 3-D view. And 91.8% of the shifts are located in the 5×5 square area. The large displacements located in the boundary correspond to the incorrectly extracted SPs caused by corrupted ridge/valley structures.

Fig. 17b is the histogram of the displacement of consistency that is computed by $\sqrt{x_t^2 + y_t^2}$. The mean displacement between the reference SP and matching SP is 3.18 in pixels, and the standard deviation is 3.16 in pixels. There are 89.7% displacements less than the mean plus one standard deviation, that is, less than 6.34 pixels. This result shows that the displacements of the most of the detected SPs are within one ridge width, that is, the extracted SPs have high consistency. Furthermore, it indirectly demonstrates that the proposed OF estimation algorithm is robust.

Table 3 shows the consistent comparisons among the proposed method, template matching-based method [19] and shape analysis-based method [15]. The positions of reference SPs are extracted manually in the last two methods, and the displacements are calculated between the manually detected SPs (HDSP) and algorithm-based SPs (OFSP) in the identical fingerprint image. Since the manually detected reference SP is hard to provide convincing landmarks, in this study, the consistency is measured by the displacement of the identical SPs between different fingerprints of the same fingertip based on CCM. These results confirm that the proposed method produces consistent SPs.

4.5. Computational cost

The proposed algorithms are implemented on a 2.4 GHz Core2 computer in Matlab environment. The runtimes in each stage of SP detection are shown in Fig. 18. As shown, the runtime of a Gaussian filter is dependent on the filter size. Therefore, the filter size should be reduced when satisfying the smoothing requirement. Moreover, the automatic candidate SP searching still needs to be optimized. Table 4 shows the average runtime comparison of the three OF estimation methods over entire dataset (880 images). Same as the proposed method, the conventional method [29] and the weighted method [31] are all coded by the author and implemented in Matlab. The same efforts have been given to these algorithms for their optimization. The weighted method has the identical computational complexity as that of the conventional method, but takes much longer runtime due to the computation of the covariance of the four neighboring

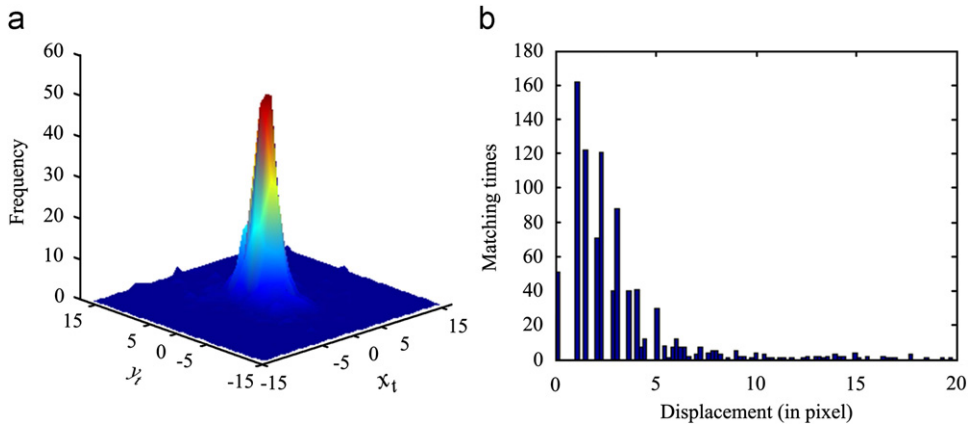

Fig. 17. (a) Distribution of displacement in 3-D and (b) histogram of the displacement.

Table 3
Consistency comparison (measured in pixels), where *M* and *STD* refer to mean and standard deviation of displacement, respectively.

Approach	$M \pm N$	Comments
Template matching-based [19]	5 ± 3	HDSP versus OFSP in the same fingerprint
Shape analysis-based [15]	$N/A \pm 6.39$	HDSP versus OFSP in the same fingerprint
Proposed	3.16 ± 3.18	Identical OFSPs in different fingerprints

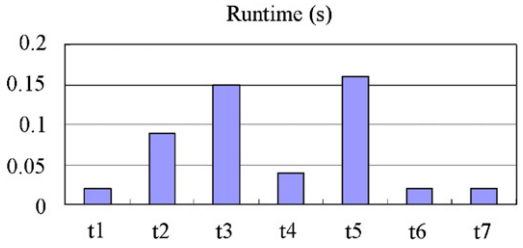

Fig. 18. Runtime of SP detection: (t1) gradient vectors filtering, (t2) coherence data filtering, (t3) orientation filtering, (t4) the computation of magnitude of angular gradient, (t5) finding the local peak point in magnitude plane, (t6) validation of candidate SPs by NPI, and (t7) validating by BPNN per candidate SP.

Table 4
Average runtime comparison for the OF estimation over the entire dataset, w_g, w and $M \times N$ refers to the window size of Gaussian filter in three scales (7, 31, 61), the block size in other two methods and the image's height by width, respectively.

Method for the OF estimation	Runtime (s)	Computational complexity
The conventional method [29] (block size: 24×24 pixel)	0.10	$O((M \times N)/w^2)$
The weighted method [31] (block size: 24×24 pixel)	0.19	$O((M \times N)/w^2)$
The proposed method (pixel-wise OF)	0.26	$O(M \times N \times w_g)$

blocks. Although the runtime of the proposed method is longer than the other two methods, it is still short enough to be applied into real-time fingerprint recognition and it is worth to sacrifice a little runtime to achieve greater accuracy.

Because its un-optimized searching algorithm, finding peak points in the magnitude plane takes the longest runtime. It is important to note here that for this part of the process, the execution time is not an important issue, since it is not an optimized compiled code. Certainly, better results can be expected from faster optimization algorithms, especially for the candidate SP extraction algorithm. Some of these modifications are being further studied and tested at present.

5. Conclusions

This paper presents a new pixel-level singular point detection method for fingerprints via multi-scale Gaussian filtered orientation field. The multi-scale Gaussian filtering increases the robustness and the resolution of the orientation field, thus, results in consistent pixel-level singular point detection. The rationale behind the pixel-level orientation field estimation is identical to the gradient-based method, however, the convolution operations enhance the accuracy and robustness of the orientation field estimation than the block summation with post smoothing processing in conventional methods. Moreover, the proposed method utilizes a coarse-to-fine strategy to extract the singular points. Firstly, the candidate singular points which are the discontinuous points in the orientation field are detected from the robust pixel-level orientation field, then, the nested Poincare indexing and the local feature-based classification are used to verify and remove the false singular points. The combination of testing in the orientation field domain and the local-feature domain extremely reduces the false singular points. In addition, a cross correlation matching-based performance evaluation of singular point detection results in objective performance evaluation for the proposed method. Furthermore, since the singular points are detected in pixel-level, the proposed method is able to detect very closely neighboring singular points, for instance, two close cores and core-delta pairs.

The main contributions of this paper consist of: (i) a pixel-wise angular gradient-based candidate singular point extraction method, (ii) a cascade framework comprised of NPI and local feature-based classification, and (iii) a cross correlation matching-based quantitative performance evaluation for the accuracy of the orientation field and singular points. The proposed method will produce biased results in severely smudged areas as the proposed method utilizes only the local information. Future works will include the combination of the global model-based orientation field with the proposed method to predict and detect singular points.

Acknowledgment

This work was supported by the Korea Science and Engineering Foundation (KOSEF) through the Biometrics Engineering Research Center (BERC) at Yonsei University (no. R112002105080010 (2009)).

References

[1] L. Wang, M. Dai, Application of a new type of singular points in fingerprint classification, Pattern Recognition Letters 28 (2007).
[2] C.H. Park, H. Park, Fingerprint classification using fast Fourier transform and nonlinear discriminant analysis, Pattern Recognition 38 (2005) 495–503.
[3] K. Karu, A.K. Jain, Fingerprint classification, Pattern Recognition 29 (1996) 389–404.
[4] M. Kawagoe, A. Tojo, Fingerprint pattern classification, Pattern Recognition 17 (1984) 295–303.
[5] A.K. Jain, S. Prabhakar, L. Hong, A multichannel approach to fingerprint classification, IEEE Transactions on Pattern Analysis and Machine Intelligence 21 (1999) 348–359.
[6] G. Drets, H. Liljenström, Fingerprint sub-classification and singular point detection, International Journal of Pattern Recognition and Artificial Intelligence 12 (1998) 407–422.
[7] R. Cappelli, A. Lumini, D. Maio, D. Maltoni, Fingerprint image reconstruction from standard templates, IEEE Transactions on Pattern Analysis and Machine Intelligence 29 (2007) 1489–1503.
[8] P.R. Vizcaya, L.A. Gerhardt, A nonlinear orientation model for global description of fingerprints, Pattern Recognition 29 (1996) 1221–1231.
[9] B.G. Sherlock, D.M. Monro, A model for interpreting fingerprint topology, Pattern Recognition 26 (1993) 1047–1055.
[10] S. Chikkerur, N. Ratha, Impact of singular point detection on fingerprint matching performance, Presented at Fourth IEEE Workshop on Automatic Identification Advanced Technologies, 2005.
[11] E.R. Henry, Classification and Uses of Finger Prints, George Routledge and Sons, London, 1900.
[12] ISO/IEC, International Standard ISO/IEC 19794-2 Information Technology—Biometric data Interchange Formats—Part 2: Finger Minutiae Data, 2005.
[13] K. Nilsson, J. Bigun, Localization of corresponding points in fingerprints by complex filtering, Pattern Recognition Letters 24 (2003) 2135–2144.
[14] X. Wang, J. Li, Y. Niu, Definition and extraction of stable points from fingerprint images, Pattern Recognition 40 (2007) 1804–1815.
[15] C.-H. Park, J.-J. Lee, M.J.T. Smith, K.-H. Park, Singular point detection by shape analysis of directional fields in fingerprints, Pattern Recognition 39 (2006) 839–855.
[16] L. Fan, S. Wang, H. Wang, T. Guo, Singular points detection based on zero-pole model in fingerprint image, IEEE Transactions on Pattern Analysis and Machine Intelligence 30 (2008) 929–940.
[17] Y. Wang, J. Hu, D. Phillips, A fingerprint orientation model based on 2D Fourier expansion and its application to singular-point detection and fingerprint indexing, IEEE Transactions on Pattern Analysis and Machine Intelligence 29 (2007) 573–585.
[18] A.M. Bazen, S.H. Gerez, Systematic methods for the computation of the directional fields and singular points of fingerprints, IEEE Transactions on Pattern Analysis and Machine Intelligence 24 (2002) 905–919.
[19] K. Nilsson, J. Bigun, Registration of fingerprints by complex filtering and 1D projections of orientation images, in: Lecture Notes in Computer Science, vol. 3546, 2005, pp. 171–183.
[20] S.C. Dass, Markov random field models for directional field and singularity extraction in fingerprint images, IEEE Transactions on Image Processing 13 (2004) 1358–1366.
[21] W. M. Koo, A. Kot, Curvature-based singular points detection, Presented at International Conference on Audio- and Video-Based Biometric Person Authentication, 2001.
[22] M.R. Rahimi, E. Pakbaznia, S. Kasaei, An adaptive approach to singular point detection in fingerprint images, AEU—International Journal of Electronics and Communications 58 (2004) 367–370.
[23] M.A. Oliveira, N.J. Leite, A multiscale directional operator and morphological tools for reconnecting broken ridges in fingerprint images, Pattern Recognition 41 (2008) 367–377.
[24] A.K. Jain, S. Prabhakar, L. Hong, S. Pankanti, Filterbank-based fingerprint matching, IEEE Transactions on Image Processing 9 (2000) 846–859.
[25] C. Jin, H. Kim, High-resolution orientation field estimation based on multi-scale Gaussian filter, IEICE Electronics Express 6 (2009) 1781–1787.
[26] S. Huckemann, T. Hotz, A. Munk, Global models for the orientation field of fingerprints: an approach based on quadratic differentials, IEEE Transactions on Pattern Analysis and Machine Intelligence 30 (2008) 1507–1519.
[27] J. Zhou, J. Gu, A model-based method for the computation of fingerprints's orientation field, IEEE Transactions on Image Processing 13 (2004) 821–835.
[28] A.M. Bazen, N.J. Bouman, R.N.J. Veldhuis, A multi-scale approach to directional field estimation, Presented at 15th Annual Workshop on Circuits, Systems and Signal Processing, Veldhoven, the Netherlands, 2004.
[29] A.R. Rao, R.C. Jain, Computerized flow analysis: oriented texture fields, IEEE Transactions on Pattern Analysis and Machine Intelligence 14 (1992) 693–709.
[30] Y. Mei, H. Sun, D. Xia, A gradient-based combined method for the computation of fingerprints' orientation field, Image and Vision Computing 27 (2008) 1169–1177.
[31] Y. Wang, J. Hu, F. Han, Enhanced gradient-based algorithm for the estimation of fingerprint orientation fields, Applied Mathematics and Computation 185 (2007) 823–833.
[32] Z.M. Kovčs-Vajna, R. Rovatti, M. Frazzoni, Fingerprint ridge distance computation methodologies, Pattern Recognition 33 (2000) 69–80.
[33] Y. Chen, S.C. Dass, A.K. Jain, Fingerprint quality indices for predicting authentication performance, in: Lecture Notes in Computer Science, vol. vol. 3546, 2005, pp. 160–170.
[34] D. Maio, D. Maltoni, R. Cappelli, J.L. Wayman, A.K. Jain, FVC2000: fingerprint verification competition, IEEE Transactions on Pattern Analysis and Machine Intelligence 24 (2002) 402–412.
[35] D.W. Patterson, Artificial Neural Networks, Prentice-Hall, 1995.
[36] V.N.M. Aradhya, A. Rao, G.H. Kumar, A multi-lingual character recognition system based on subspace methods and neural classifiers, Workshop on Image and Speech Processing, IIT Guwahati, India, 2007, pp. 16–21.
[37] V. Vapnik, The Nature of Statistical Learning Theory, New York, 1995.

CHANGLONG JIN completed his BS at Jilin Institute of Technology, China, in the Department of Automation, and his MS in the Department of Computer Science and Technology at Yanbian University, China, in 1994 and 2005, respectively. He is currently pursuing a PhD in the Computer Vision Lab of the Graduate School of Information & Communication Engineering at Inha University. His study includes pattern recognition, biometrics, and image processing.

HAKIL KIM received a BS in Control and Instrumentation Engineering from Seoul National University, Korea, in 1983, and MS and PhD degrees in Electrical Engineering from Purdue University in 1985 and 1990, respectively. He is currently a Professor at the School of Information & Communication Engineering in Inha University, Incheon, Korea, and a member of the Biometrics Engineering Research Center at Yonsei University, Seoul, Korea. He has been actively participating in the WG5 (testing and reporting) of ISO/IEC JTC1-SC37 and ITU-T/SG17 WP2/Q.8 telebiometrics as a rapporteur.